On sub-micrometre inclusions in diamond coat: crystallography and composition of ankerites and related rhombohedral carbonates

J. C. WALMSLEY* AND A. R. LANG

H. H. Wills Physics Laboratory, University of Bristol, Tyndall Avenue, Bristol BS8 1TL, UK

Abstract

Crystallographic studies of micro-inclusions in diamond coat, carried out by analytical electron microscopic techniques, show that structures possessing rhombohedral symmetry form a significant fraction of the population of well-crystallised particles. They are, however, less frequent than apatite or biotite, which were identified earlier by the same investigative methods. Thin-foil specimens of diamond coat were prepared by mechanical fine-polishing, and subsequently ion-beam milling, sawn and polished plates of coated diamonds oriented parallel to (100) or (110). The majority of crystalline inclusions analysed were $\leqslant 0.2$ μm in diameter. Data obtained on 15 individual inclusions, including composition analysis by energy-dispersive X-ray spectroscopy, are reported and discussed. The a-axis of the hexagonal unit cell, and the c/a ratio, were determined for all specimens, and are believed to be accurate to $\approx 1\%$ in most cases. In 12 out of 15 specimens, the cations with $Z \geqslant 11$ identified comprised substantially only Mg, Fe and Ca. Values of a in these specimens ranged from 4.81 to 4.92 Å; and for three of them the space group $R\bar{3}$, corresponding to the dolomite structure, was positively identified. These crystals are classed as ankerites. Representative Mg:Fe:Ca ratios in the ankerites are 28:18:54, with cell dimensions $a = 4.87$ Å, $c/a = 3.37$. The ankerites contained small amounts of Ba, typically 1–3%, and smaller amounts of Sr, typically 0.2–2%. Three out of the 15 specimens contained >10% Ba. In two of these, Ba and Ca concentrations were roughly equal, and in one of the two, which had cell parameters $a = 5.11$ Å, $c/a = 3.50$, the space group symmetry $R\bar{3}c$, corresponding to the calcite structure, was verified.

KEYWORDS: ankerite, carbonates, diamond coat, inclusions.

Introduction

THE recent paper by Guthrie *et al.* (1991) concerning micro-inclusions in diamond coat prompts us to put on record certain positive crystallographic identifications of mineral species discovered among the sub-micrometre-sized bodies present in diamond coat. The findings here reported constitute significant quantitative extensions to the observations described by Guthrie *et al.*, and they were obtained via experimental procedures exemplifying a rather stricter approach in the matter of mineral identification. For a crystal species so varied in defect and

impurity content as natural diamond, the modification known as 'coated' comprises a relatively easily distinguishable class, the variety IV in the classification of Orlov (1977). Coated diamonds display a clearly visible transition from a transparent 'core', which is often of gem quality, to a 'coat' that is translucent but not transparent. Coated diamonds occur widely, but their relative abundance varies much from source to source. The principal differences between core and coat can be summarised briefly in the following list. (1) Diamond coat contains a dense population of non-diamond bodies, mostly below optical microscopic resolution limit in size. These destroy the transparency, though their volume fraction probably rarely exceeds one per cent (Custers, 1950; Kamiya and Lang, 1965). (2) At the core–coat boundary there is a sharp transition from normal

* Present address: Nuclear Electric, Berkeley Nuclear Laboratories, Berkeley, Gloucestershire GL13 9PB, UK.

(and often quite perfect) growth on {111} facets to a dislocation-rich, columnar mode of growth (Kamiya and Lang, 1965; Machado et al., 1985). (3) The commonest identified impurity element in diamonds, nitrogen, may be either more or less abundant in the coat relative to the core in any coated diamond, but whenever a qualitative difference in the nitrogen-dependent infrared absorption spectra between core and coat is observed, it is in the direction indicating a less advanced state of nitrogen aggregation in the coat; and core and coat have different isotopic signatures (Boyd et al., 1987). (4) Strong non-diamond contributions to the infrared absorption spectrum of diamond coat are observed (Chrenko et al., 1967), and have recently been comprehensively studied (Navon et al., 1988); H_2O and carbonate ions are among the principal non-diamond contributions. (5) Microanalytical techniques such as electron probe microanalysis and secondary ion mass spectroscopy applied to diamond coat (Navon et al., 1988) find, for example, a relative richness in potassium that, in addition to the abundance of volatiles, chemically distinguishes the non-diamond bodies in diamond coat from the larger-sized mineral inclusions (diameters greater than ≈ 100 μm) that have been much studied in normal diamonds, and upon which current ideas on diamond genesis are largely based (Harris, 1980; Meyer, 1987; Kesson and Ringwood, 1989).

The differences listed above all point towards core and coat having grown under significantly different environments. Since coated diamonds form a not insignificant proportion of all natural diamonds, investigation of the mineralogy of coat micro-inclusions deserves an important place in studies of diamond origins. But whereas the larger inclusions familiar in normal diamond growth can be examined individually by single-crystal X-ray diffraction methods, and sometimes by optical crystallographic methods also, the identification of *individual* sub-micrometre-size crystals in diamond coat can only be carried out by analytical electron microscopic techniques that allow both the composition and the crystallography of the particle to be established. Such joint diffraction and compositional analysis has provided positive identifications of apatite (Lang and Walmsley, 1983) and biotite (Walmsley and Lang, 1992a) among minerals present in diamond coat. Crystallographic investigations particularly relevant to the carbonate inclusions discussed by Guthrie et al. (1991) are presented below. They concern ankerite, a Mg–Ca–Fe carbonate that has the dolomite structure, and Ca–Ba carbonates having the calcite structure.

Experimental procedure

Specimen selection and preparation. In continuing research on defects in coated diamonds we make use of a range of assessment methods to assist selection of specimens likely to contain features of microstructural interest, e.g. infrared absorption spectroscopy, optical and cathodoluminescence microscopy, and X-ray topography (Walmsley, 1981). Some scores of coated diamonds from Zaïre have been examined. Most of the specimens were initially in the form of half-octahedra, obtained by dividing a coated octahedron into two by a saw cut parallel to a central cube plane. For more detailed study, slices were cut from these specimens, either parallel to the existing cube-orientation sawn surface, or normal to it to produce a slice parallel to (110). (The latter orientation is particularly useful for examining the core–coat transition since its surfaces are normal to two pairs of octahedral growth surfaces; Lang et al., 1992). We used traditional sawing and polishing methods: sawing with the edge of a rotating thin annular bronze blade and polishing on a rotating cast-iron 'scaife', both blade edge and scaife surface being charged with fine diamond powder soaked in olive oil (Bruton, 1978). Using the scaife, slices several mm^2 in area could be polished to thicknesses of only 30 to 50 μm in preparation for ion-beam milling down to electron-transmitting thicknesses. Any significant departure of slice orientations from (001) or (110) could be measured, if need be, by X-ray goniometry. It follows that all specimen foils prepared for transmission electron microscopy (TEM) were in pre-determined crystallographic orientation. They also bore a known geometrical relation to the local core–coat boundary and the direction of crystal growth.

The argon-ion-beam milling was carried out on both sides of the specimen, which was clamped between a pair of thin molybdenum discs having centrally punched 1 mm-diameter holes through which the ion beam impinged upon the specimen. The discs were continuously rotated in their own plane, with which the ion beam made an angle of 30°. The usual argon ion energy of 5 kV was reduced to 3 kV for the final stage of thinning in the hope of reducing ion beam damage to inclusions. Total specimen thinning rates were between 1 and 1.5 μm per hour.

Analytical electron microscopy. The TEM experiments were performed with a Philips EM430 instrument operating up to 300 kV. The results here reported were obtained at 200 kV, an energy adequate to give good contrast images with diamond thicknesses >1 μ and offering a

favourably low rate of electron beam damage to inclusions. A Philips 'tilt-rotate' specimen holder was used, which allowed complete rotation of the specimen in its own plane and a ±60° tilt about an axis in the specimen plane. For all bright-field and dark-field images of importance, the diffraction conditions applying were put on record by photographing the diffraction pattern. Lattice parameters of inclusions were derived from interplanar spacings measured relative to calibrating diffraction patterns from the diamond matrix.

Information on inclusion composition was obtained by energy-dispersive X-ray spectroscopy (EDS). The X-ray energy range from 0 to 20 kV was covered. Hence elements with atomic number Z greater than 44 (whose $K\alpha$ X-ray energies exceed 20 keV) were identified by their L-series X-ray emissions. Absorption by the Be window on the X-ray detector prevented detection of elements lighter than Na, $Z = 11$. In a typical inclusion analysis, the counting rate over the 20 keV range would be about 10^3 per second, much higher than the 20–200 counts per second quoted for the analyses by Guthrie et al. (1991). A measure of the statistical accuracy of our analyses can be derived from the magnitude of the integrated photon count in the $K\alpha$ peak of the dominant element, which was Ca in the case of carbonates. The total count, N, of $CaK\alpha$ photons detected was typically 3×10^4, for which the relative variation, $N^{-1/2}$, is only 0.6%. Relative concentrations of elements from Mg ($Z = 12$) to Fe ($Z = 26$) were found from the areas of their $K\alpha$ peaks (after background subtraction) multiplied by the sensitivity factor for the radiation concerned, the Cliff-Lorimer k-factor (Cliff and Lorimer, 1975). A curve of the variation of k with Z in our apparatus was derived from the EDS spectrum given by a standard biotite specimen in the form of a cleavage flake thin enough to be electron-transmitting. Its composition had been determined from a calibrated electron-probe X-ray spectroscopic microanalysis. For assaying Ba and Sr concentrations relative to Ca, the k-factors of BaL, SrK and SrL radiations relative to that of SK radiation were found from spectra of very fine particles (<1 μm diameter) of $BaSO_4$ and $SrSO_4$, and were combined with the known sulphur/calcium sensitivity ratio.

Results

Ankerite identification. Crystalline micro-inclusions that were discovered to be rhombohedral carbonates of ankerite type attracted attention by virtue of the characteristic symmetry of the diffraction patterns they produced when the incident electron beam direction coincided with their trigonal axis, together with the simplicity of their EDS spectra, which substantially contained only the elements Mg, Ca and Fe. It was helpful in the investigation that strong, well-ordered diffraction patterns could be obtained from these carbonates. The following TEM images and diffraction patterns illustrate the procedure leading to crystallographic identification of ankerite. The bright-field micrograph, Fig. 1, shows at its centre an ankerite crystal, overall size 250 nm. In this view it appears irregularly-shaped. Its image appears very dark on the print because the crystal is diffracting strongly. The blackness is in fact modulated by thickness extinction contours, evidence of the major contribution of diffraction contrast to the image of the crystal. The diamond matrix, on the other hand, is not oriented to give any strong Bragg reflections; and the contrast in its image arises almost totally from absorption differences. The bright, rounded patch abutting the upper right edge of the ankerite crystal represents a substantially eroded cavity in the diamond. Other cavities showing light on the print (and thus presumed to be now empty) are sufficiently un-eroded to retain some flat diamond {111} bounding surfaces. Cavities of this type connect with the ankerite crystal on its upper left and bottom right. Non-diamond material (showing dark) is retained in a number of small, totally-enclosed volumes seen in the upper part of the field, and also in the larger, partially-filled and partially-faceted cavity in the lower part of the field. The overall diamond foil thickness in Fig. 1 is 0.7 μm. The foil orientation is roughly parallel to diamond (110), which enables some {111} facets to be seen edge-on, enclosing the characteristic acute angle of 70.5°.

Fig. 2 is the diffraction pattern given by the ankerite crystal oriented as in Fig. 1. It is very close to the [0001] zone axis pattern (adopting hexagonal indexing); a small deviation of the incident electron beam from exact coincidence with this axis causes some inequality in strengths of symmetrically equivalent reflections. [In this report, images and diffraction patterns are reproduced in correct relative orientation, and both are printed as viewed looking down on the fluorescent screen of the electron microscope. Thus in Fig. 1, taking the crystal axis [0001] pointing towards the observer, the electron beam is travelling in the [000$\bar{1}$] direction.]

Fig. 3 shows sections of the reciprocal lattice of the hexagonal unit cell (which for this crystal has an axial ratio, c/a, of 3.36). Only reflections $hkil$ with $-h + k + l = 3n$ are possible because of the
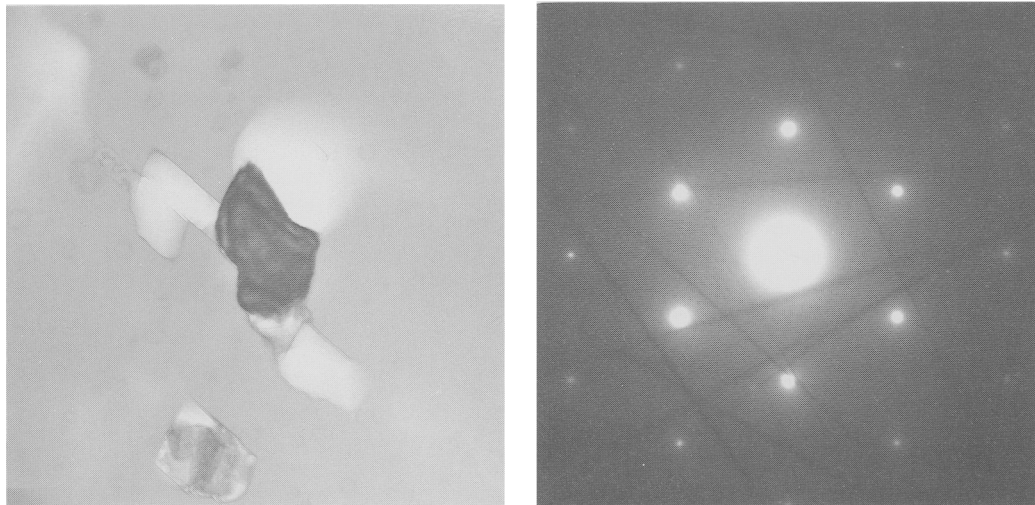
FIGS. 1 and 2. Fig. 1 (*left*). Bright-field micrograph of ankerite micro-inclusion within diamond. Ankerite appears very dark due to strong diffraction contrast. Field width 0.8 μm. Fig. 2 (*right*). The [0001] zone axis diffraction pattern given by the ankerite crystal oriented as in Fig. 1. The reflections are identifiable from the plan of the hki0 reciprocal lattice layer shown in the top part of Fig. 3. The strong innermost ring of six reflections are of $11\bar{2}0$ type. The next ring of six, much weaker, are of $3\bar{3}00$ type; and the outermost, weaker still, are $22\bar{4}0$ type. Dark lines crossing this and other diffraction patterns are Kikuchi lines from the diamond matrix.

rhombohedral symmetry of the structure. The diffraction patterns shown in Figs. 2, 5(*a*) and 6(*a*) can be indexed with the help of Fig. 3. The Ewald sphere is sufficiently flat to be represented by a plane within the volume of reciprocal space concerned in the diffraction patterns. By rotating the specimen about the $[1\bar{1}20]$ direction (which is vertical in the plane of Figs. 1 and 2), several informative zone axis diffraction patterns were brought into view and photographed. After a rotation bringing the ankerite $[2\bar{2}01]$ axis to point towards the observer, the crystal silhouette changes greatly. A well-developed cleavage rhomb facet is now seen edge-on (Fig. 4). Diffraction contrast of ankerite relative to diamond matrix is again very strong in Fig. 4, assisted by strong Bragg reflections from the cleavage plane. Cleavage plane indices (which are {100} in rhombohedral axes defined by cleavage rhomb edges) are {211} in the X-ray structural rhombohedral axes and $\{10\bar{1}4\}$ in the corresponding hexagonal axes used here. Note that the specimen rotation between the settings of Figs. 1 and 4 changes the corner angles of silhouettes of diamond {111}-faceted cavities to become near right angles in Fig. 4 because in this figure the diamond is viewed roughly parallel to a cube axis. Fig. 5(*a*) shows the diffraction pattern corresponding to the image in Fig. 4; Fig. 5(*b*)

identifies reflections. The contrast of diffraction spots is less than in Fig. 2 in consequence of the high specimen tilt, which increases the specimen thickness along the electron beam direction from 0.7 μm to 1 μm.

Among other diffraction patterns recorded, the most significant was that obtained with the specimen tilted to align the ankerite $[1\bar{1}02]$ direction with the incident beam. It is reproduced in Fig. 6(*a*), with identification of reflections in Fig. 6(*b*). This is the key pattern for distinguishing between the calcite structure, space group $R\bar{3}c$, and the dolomite structure, space group $R\bar{3}$ (Bragg and Claringbull, 1965). In space group $R\bar{3}c$, reflections $1\bar{1}01$ and $02\bar{2}1$ are forbidden, but in space group $R\bar{3}$ they are allowed. However, these reflections are rather weak in dolomite, and even weaker in ankerite (Graf, 1961; Howie and Broadhurst, 1958). Reflections $\bar{1}101$, $02\bar{2}1$ and their symmetrical equivalents do appear, weakly, in the Fig. 6(*a*) diffraction pattern; and they demonstrate the symmetry corresponding to the dolomite structure. Lattice parameter and composition measurements on this ankerite crystallite (specimen no. 2) are included in Table 1, discussed below. However, it is very relevant to the question of the mineral species identification of specimens such as this to note the similarity of its lattice parameters ($a = 4.87$ Å, $c/a = 3.36$) to

those ($a = 4.819$ Å, $c/a = 3.341$) of an ankerite of roughly similar composition studied by Howie and Broadhurst (1958).

Crystallographic and composition data for rhombohedral carbonates. Having explained above how crystallographic data were obtained for a typical ankerite particle, experiments on

FIG. 4. Bright-field micrograph of ankerite crystal recorded after rotating specimen $\approx 45°$ relative to its orientation in Fig. 1: rotation axis [$\bar{1}\bar{1}20$], vertical in the plane of the image. In this image ankerite [$2\bar{2}01$] points towards the observer, and a cleavage rhomb facet is seen edge-on, bounding the ankerite crystal on the left.
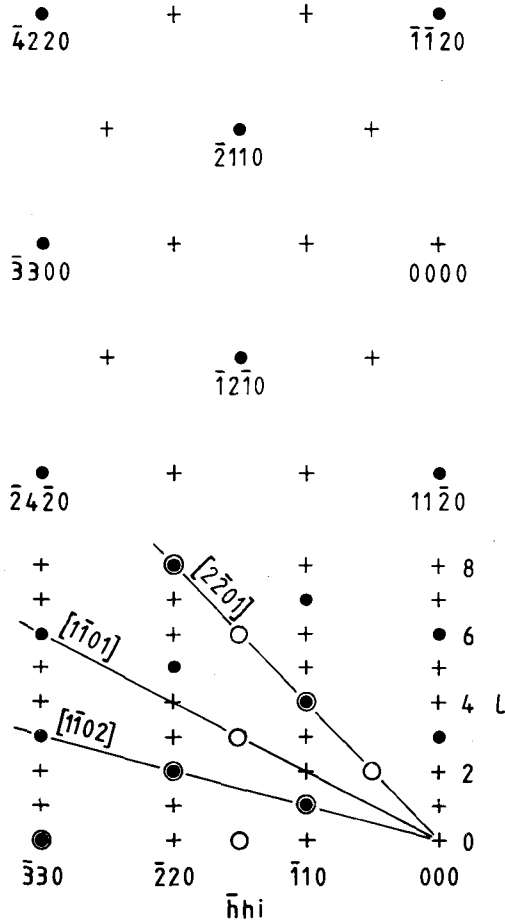

FIG. 3. Sections of reciprocal lattice corresponding to the direct-lattice hexagonal cell with $c/a = 3.36$. Above: plan of the $hki0$ layer. Below: the $\bar{h}h0l$ section for the range $h = 0$ to 3 and $l = 0$ to 8. In the $hki0$ layer and $\bar{h}h0l$ section, allowed reflections from a rhombohedral crystal structure are identified by large dots. On the $\bar{h}h0l$ section, the sloping lines show intersections with reciprocal lattice planes normal to the direct-lattice directions indicated. Reflections in the $\bar{h}h0l$ plane that have been recorded with significant intensity are shown by encircled dots. Some other observed reflections, not lying in the $\bar{h}h0l$ section, are indicated by projections of their reciprocal lattice points on to the $\bar{h}h0l$ plane (open circles).
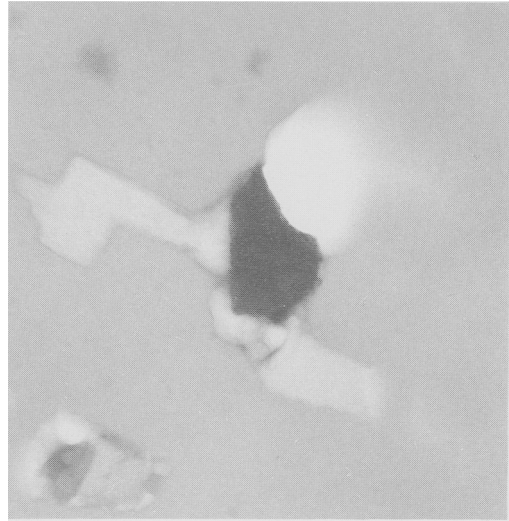
other specimens can be summarised in the findings represented in Table 1. The 15 specimens included in the Table, which are numbered in order of increasing Ba content, can be taken as representing a fair sample of rhombohedral carbonate micro-inclusions in diamond coat. Their diameters ranged between 0.1 and 0.2 μm, except specimens 7 and 11 (diameters 0.4 μm) and specimen 13 (diameter 1 μm). The crystallographic data will be discussed first, the EDS analyses later. When definitive evidence on the space group was available from photographs of reciprocal lattice layers similar to that shown in Fig. 6, the result is indicated in Table 1 by a D for dolomite structure and C for calcite structure. Combining the evidence on lattice parameters, symmetry and compositions, it is reasonable to assume that all specimens 1 to 13 possessed the dolomite structure. Specimen 15 gave excellent strong and sharp diffraction patterns (better than those of specimen 2 illustrated above), and there was no doubt as to the complete absence of reflections $\bar{1}101$, $02\bar{2}1$, etc. The specimen was therefore assigned to the calcite space group $R\bar{3}c$; and this is considered the more likely space group for specimen 14 also.

The hexagonal-cell a-axis dimensions were derived directly from the $11\bar{2}0$ or $22\bar{4}0$ interplanar spacings for all specimens except specimen 11.
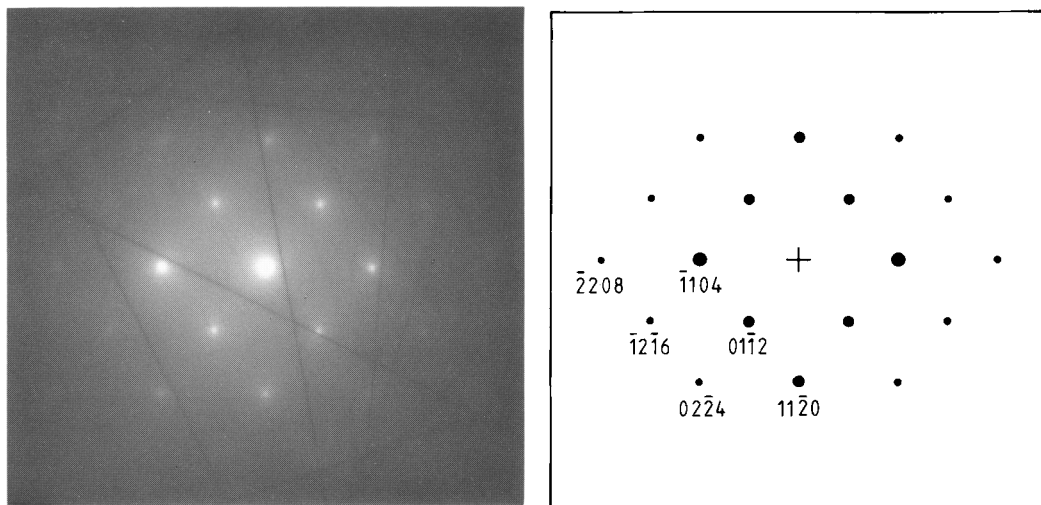
Fig. 5. (*a, left*). Ankerite [$2\bar{2}01$] zone axis diffraction pattern. (*b, right*). Key to reflections in (*a*).
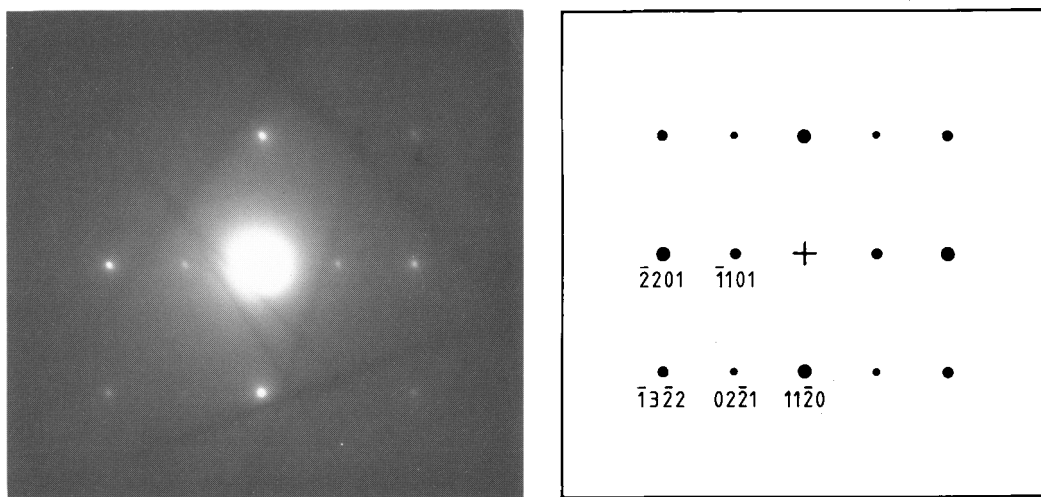

Fig. 6. (*a, left*). Ankerite [$1\bar{1}02$] zone axis diffraction pattern. (*b, right*). Key to reflections in (*a*).

The most precise measurements were obtained when diameters between the diffraction spots of the higher-order reflections, $\pm 22\bar{4}0$, were easily measurable. Sharp spots of sufficient strength for such measurement were produced by specimens 4, 7, 8, 10 and 15. In their cases the reproducibility of diameter measurement was about 2 parts in 10^3; and differences of 0.01 to 0.02 Å in *a*-values (which are quoted to 0.01 Å in Table 1 for all but one specimen) might then be meaningful. In other specimens the uncertainty of differences

is at a higher level, but is less than 0.05 Å except in the case of specimen 12. As regards absolute values of *a*, all depend upon the camera calibration adopted, which is believed to be accurate to between 0.5 and 1%. However, displacements of diffraction spots by electron refraction dependent upon the crystallite shape, and of a magnitude not readily quantifiable, might be present in the diffraction patterns of the inclusions. Such could influence both *a* and *c/a* measurements; but the additional uncertainty thereby imposed on

Table 1. Crystallographic and composition data for rhombohedral carbonate inclusions

(Hexagonal unit cell parameters and relative atomic concentrations)

Specimen	1	2	3	4	5	6	7	8	9	10	11	12	13	14	15
$a/Å$	4.89	4.87	4.84	4.86	4.90	4.81	4.89	4.92	4.88	4.88	4.87	4.9	4.77	5.06	5.11
c/a	3.3(1)	3.36	3.38	3.37	3.34	3.42	3.(1)	3.34	3.38	3.39	3.35	3.2	3.40	3.58	3.50
Structure		D		D							D		D		C
Mg	23(24)	26(27)	23(25)	12	17	24	28(32)	16	22	22	15	12	22	10	4
Al	2	1	2	-	2	-	2	<1	1	1	4	<1	1	-	-
Si	-	1	1	-	11	8	4	15	14	6	4	4	-	4	-
P	1	-	5	19	4	-	-	-	2	-	8	-	-	-	2
S	-	-	-	-	-	-	-	-	-	-	3	-	9	-	3
Cl	-	1	1	-	<1	-	2	-	<1	-	-	-	2	-	5
Ca	54(56)	50(52)	50(55)	53	48	34	49(56)	50	42	52	46	62	43	41	35
Fe	19(20)	20(21)	18(20)	14	17	32	11(12)	16	16	15	15	16	10	3	9
Sr	<1	<1	<1	1	<1	<1	<1	<1	<1	<1	2	<1	1	1	1
Ba	<1	<1	<1	1	1	1	1	2	2	3	3	6	11	40	40
Sr/Ca	0.004	0.002	0.003	0.016	0.011	0.068	0.009	0.008	0.014	0.011	0.043	0.010	0.035	0.040	0.041
Ba/Ca	0.010	0.012	0.012	0.027	0.028	0.029	0.030	0.035	0.041	0.053	0.070	0.093	0.27	0.99	1.1

them is nominally assessed to be not greater than a small fraction of 1%.

Diffraction patterns including the $000l$ row of reflections as well as reflections from planes with $l = 0$ were not recorded. Accordingly, determination of the c/a ratio was obtained from the ratio of spacings of planes whose reciprocal vectors had, respectively, a large and a small (preferably zero) component parallel to the c-axis. These spacing measurements were always made on the same film. A precision of measurement of c/a better than 1% (excluding possible refraction effects considered above) is believed to apply in the case of specimens 4, 5, 6, 8 and 10, and of between 1% and 2% in the others (except specimens 1, 7 and 12, for which the accuracy was poor, due to reflections being unsharp in the case of specimen 12, and having indices giving ill-conditioned equations for deriving c/a in the case of specimens 1 and 7).

Turning to the EDS spectra, first to be considered are some general matters concerning the interpretation and presentation of the findings. The diamond specimens were supported on copper electron microscope grids. Consequently,

substantial CuK radiation components were always present in the spectra. Fortunately, the energies concerned (Cu$K\alpha$ = 8.04 keV, Cu$K\beta$ = 8.90 keV) do not interfere with the K or L emissions of any other elements of present concern. The fractional contribution to the total spectrum that came from radiations not emanating from the inclusion itself (and therefore to be disregarded) varied from specimen to specimen, naturally being greater when the inclusion was very small. Requiring more attention than the CuK emissions was a small variable contamination of the spectra by MoK and MoL emissions, generated primarily by molybdenum-containing electron-beam apertures in the electron microscope, but also possibly arising from molybdenum on the specimen that had been sputtered off the edges of the holes in the molybdenum discs holding the specimen. The energies of Mo$L\alpha$ and S$K\alpha$ radiations are both close to 2.3 keV. However, the Mo$K\alpha$ peak (17.4 keV) occurs well separated from other peaks, and if it appeared with measurable intensity then an appropriate subtraction was made from the 2.3 keV peak. In practice, discrimination between spectra that

contained a significant sulphur signal (specimens 11, 13 and 15) and those that did not was quite clear. Another spectral occurrence explicable as an experimental artefact was that nine out of the 15 spectra indicated trace presence of argon, which is believed to have come from implantation into the inclusion during the ion-beam thinning operation.

A serious spectral interference arising in all cases was that between SrLα (1.81 keV) and SiKα (1.74 keV). The quality of the spectra was sufficiently good to enable distinction to be made between substantially different Sr/Si concentration ratios from the position of the peak, but to determine this ratio quantitatively recourse was made to the same procedure as used in establishing the relative contributions of Mo and S to the 2.30 keV peak. Fortunately, the calibration experiments performed with fine particles of SrSO$_4$ provided reliable values for both peak height and peak area ratios between SrKα and SrLα emissions. Thus, from measurement of height or area of the SrKα peak at 14.1 keV the contribution of SrLα to the observed low-energy peak could be calculated, and subtracted from it. The balance remaining was attributed to SiKα.

In Table 1, atomic concentrations are expressed as percentages of all the species quantitatively assayed in each specimen. The Sr/Ca and Ba/Ca atomic ratios are calculated from concentration estimates before rounding to the nearest percent. (The figures in parenthesis are explained below in the Discussion). Potassium is not included among elements listed since it was clearly detected in only one spectrum (specimen 7, K concentration 2%), and in trace concentration in 5 others, specimens 5, 6, 8, 12 and 13. Chlorine is listed because of its detection in seven spectra, though its concentration exceeds 1% only in specimens 7, 13 and 15. There appeared to be traces of chromium in specimens 5, 8 and 10. A trace of manganese was detected in specimens 4, 7 and 8, doubtfully in specimen 12, and at a level of ≈2% of the iron concentration in specimens 5 and 6. Fig. 7 shows the low-energy region (up to 7.5 keV) of the spectrum of specimen 11, which can be taken as representing one of those with fairly low Sr and Ba content, but also exhibiting some untypical features among the entries in Table 1. It is exceptional in having the highest Al content, and, after specimen 4, the highest P content. The contributions from SiKα and SrLα to the peak at ≈1.8 keV were assessed to be in the ratio 2:3. (The concentration ratio differs, of course, because of difference in k-factors.) In this spectrum no Ar, K, Cr or Mn were detectable. The hint of a peak at the ClKα energy (2.62 keV) is

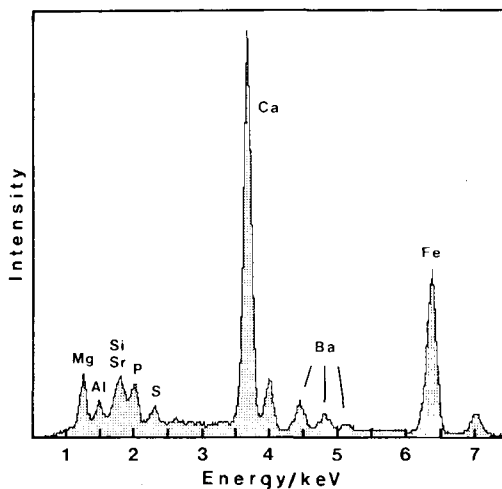
FIG. 7. Energy-dispersive X-ray spectrum of inclusion 11 in the energy range 0.5 to 7.5 keV. Intensity scale linear; CaKα peak height corresponds to 6.9 × 10^3 counts per energy channel.

insufficient to warrant stating 'Cl positively detected' in this spectrum. The area of the CaKα peak represents 53,000 CaKα photons recorded, illustrating the good counting statistics achieved. [To avoid confusion when comparing Fig. 7 with Fig. 6 of Guthrie et al. (1991), note that those authors have misplaced their 'S' label.]

Discussion

This investigation has demonstrated that dolomite and calcite structures are significant constituents of the population of micro-inclusions in diamond coat, but among crystallographically identified species they are less common than biotite or apatite. Several of the ankerite-type inclusions (including specimen 2) were found in coat-like material filling a crack in the core of a coated diamond (Walmsley and Lang, 1992b). The account of morphologies, environments and the chemical diversity of micro-inclusions in diamond coat presented by Guthrie et al. accords well with the experience underlying our investigation. Their description, and discussions of the geological implications of the chemistry of coat inclusions (Navon et al., 1988), need not be recapitulated in this summary, which will be confined to some further analysis of the techniques and findings in our electron microanalytical experiments.

The common occurrence of multi-particle assemblages within single cavities in the diamond host increases the chances of EDS analyses

including substance additional to that producing the diffraction pattern associated with a particular inclusion. Material in vitreous state (or that became rapidly so under the electron beam) would not be detected by diffraction contrast in its image or by a spot diffraction pattern. Fragments of amorphous material attached to a crystalline particle are not easily recognised in its image even after examination at various specimen tilts if the crystalline particle has been much eroded and/or has an irregular shape. In practice, every effort was made to ensure that the electron probe employed for EDS sampling did not extend outside the crystallite of interest. An example of the good separation of targets achieved in the EDS probing, combined with an observation of crystallographic interest, is provided by specimen 8. Here the TEM images revealed a plate of biotite lying on a cleavage-plane facet of the carbonate crystallite, the diffraction patterns verifying that biotite (001) was parallel to the carbonate ($10\bar{1}4$). However, the EDS analysis of the carbonate particle showed only a trace of potassium, an important constituent of biotite (and which does appear strongly in EDS spectra of biotite inclusions in diamond coat; Walmsley and Lang, 1992a).

Regarding EDS analysis, some spectral interferences relevant to the present work that occur when barium is detected by its L-series emissions should be noted. The strong $BaL\alpha_1\alpha_2$ pair of lines (energy 4.47 keV) will mask traces of titanium ($TiK\alpha$, 4.51 keV); and when concentration of Ba is high, its weak $L\gamma_2\gamma_3$ lines (5.82 keV) may mask traces of manganese ($MnK\alpha$, 5.89 keV). When interpreting the results presented in Table 1, it is safe to assume that the Sr and Ba reside in solid solution in the carbonate. On the other hand, in cases where phosphorus is detected, it is reasonable to infer that it is present independently, in apatite. In specimens where, apart from Mg, Fe and Ca, none of the detected elements is present with concentration greater than 5% of the total, the relative concentrations of Mg, Fe and Ca are shown separately in the Table (as percentages, in the parentheses) to indicate their proportion in the carbonates, assuming that they were the only cations contained therein. Such percentages can be corrected, where necessary, to allow for Ca separated with P in apatite. Taking the Ca : P ratio in apatite as 5 : 3, a proportionate fraction of the total Ca may be allocated to apatite. Applying this rule to specimen 3 yields Mg : Fe : Ca = 28 : 21 : 51 to replace the figures in parenthesis for the relative proportions of these cations in the carbonate. Combining these corrected figures for specimen 3 with the tabulated figures in par-

entheses for specimens 1, 2 and 7 yields the mean ratios Mg : Fe : Ca = 28 : 18 : 54. These are regarded as the typical cation ratios for ankerites in diamond coat. For comparison, the cation relative percentages in the ankerite analysed by Howie and Broadhurst (1958) were Mg 31.2, Fe 16.6, Mn 1.1 and Ca 51.1.

As explained earlier, Table 1 states inclusion compositions as relative atomic concentrations, which are expressed as percentages of all the elements listed for each particular specimen. These are the figures that come directly from the EDS analysis. They are deemed the most objective way of presenting the findings, involving no assumptions regarding chemical combination. However, atomic concentrations can be converted into oxide weight percentage to provide figures for comparison with conventional mineral analyses. This conversion applied to the dominant cations detected in the four specimens 1, 2, 3 and 7 selected as representative ankerites in diamond coat is presented in Table 2. In the case of specimen 3, the oxide weight percentages are based on the atomic ratios Mg : Fe : Ca = 28 : 21 : 51 that, as explained above, allow for the fraction of Ca combined in apatite rather than carbonate. On the evidence available, it is a fair assumption that all the MgO, CaO and FeO quantities in Table 2 reside in carbonates, and so it is permissible to add a calculated CO_2 weight percentage to bring column totals up to 100%. But this addition to Table 2 must be accompanied by the reminder that the light elements carbon and oxygen were not detected in the EDS experiments performed.

Turning finally to consider the lattice parameter measurements, we deal first with the ankerite-type specimens having low Ba and Sr content, specimens 1–12. It is seen that there is a scatter of about 2% in values of a, and somewhat less in values of c/a (excluding specimens 1, 7 and 12 for which diffraction patterns suitable for good c/a measurements were not available). The origin of the scatter has not been established; possible contributory factors have been mentioned in the previous section. All the crystallites concerned

Table 2 Compositions of representative ankerites (oxide weight percentages)

Specimen	1	2	3	7
MgO	10	11	11	13
CaO	32	30	29	32
FeO	14	15	15	9
$(CO_2)_{calc}$	44	44	45	45

were in opened cavities, so they were free from hydrostatic stress. Differing amounts of electron beam damage might be considered as contributors to the parameter variations. However, care was taken to record diffraction information before performing a thorough EDS analysis, since the latter involves the higher irradiation dose on the crystallite. In fact no evidence of beam damage of the carbonates was observed either from degradation of diffraction patterns or from loss of diffraction contrast in their images. This is in contrast to biotite inclusions in diamond coat, where crystal damage during EDS analysis is significant. The four specimens 1, 2, 3 and 7, adopted as possessing representative ankerite compositions, have 4.87 Å as their mean value of a. For specimens 2 and 3 the mean c/a ratio is 3.37. Recalling the values $a = 4.810$ Å, $c/a = 3.341$ found by Howie and Broadhurst (cited earlier), it is seen that our average a and c/a values are both greater by about 1%. The higher Fe/Mg ratio and the addition of some Ba in specimens 1, 2, 3 and 7 could account for about a fifth of the increase in a. However, the 1% discrepancy is not outside the range of uncertainty in determining lattice parameters in our electron diffraction experiments. It can be concluded that agreement between the present electron diffraction measurements and the X-ray diffractometric measurement by Howie and Broadhurst is noteworthy.

Regarding the Ba-rich specimens, the lattice parameters of the verified calcite structure, specimen 15, and of specimen 14 believed to be of similar structure, may be compared with those of comparable crystals studied by Chang (1965). He found complete solid solubility in the system $BaCO_3$–$CaCO_3$ above 850 °C, and measured a and c for the disordered calcite phase at this temperature. When Ba and Ca are in equal atomic proportions, the disordered calcite phase is stable down to about 500 °C. Lattice parameters of the end members are (in Å): $BaCO_3$, $a = 5.21$, $c = 20.96$, $c/a = 4.02$; $CaCO_3$, $a = 4.98$, $c = 17.07$, $c/a = 3.43$; and with Ba and Ca in equal atomic proportions, $a = 5.10$, $c = 17.80$, $c/a = 3.49$. The corresponding lattice parameters at room temperature may be estimated from available data for the thermal expansion of calcite parallel and perpendicular to c (Touloukian et al., 1977); lowering the temperature of calcite from 850 °C to room temperature decreases c by 1.5% and increases a by 0.2%. The same changes applied to the parameters quoted above for $Ba_{0.5}Ca_{0.5}CO_3$ (which is taken as the model for specimens 14 and 15) give $a = 5.11$ Å, $c/a = 3.43$. Agreement with the a measurements for specimens 14 and 15 is good, but less so for c/a, its values exceeding 3.43

by 4% and 2% in specimens 14 and 15, respectively. For both specimens the $11\bar{2}0/\bar{1}104$ pair of interplanar spacings was measured in order to derive c/a. This pair does not give c/a ratios as precise as those derived from the $11\bar{2}0/\bar{1}108$ pair, which was recorded and measured for a number of the ankerite-type specimens. Even so, c/a values listed for specimens 14 and 15 should not be in error by more than 1 to 2%. Nevertheless, the data in Table 1 for specimens 14 and 15, especially the space group finding, are interpreted as showing that in these small crystallites a Ba-rich calcite structure has been preserved down to room temperature. No evidence has been found so far for presence of carbonates with other than the rhombohedral calcite or dolomite structures among micro-inclusions in diamond coat.

References

Boyd, S. R., Mattey, D. P., Pillinger, C. T., Milledge, H. J., Mendelssohn, M., and Seal, M. (1987) Multiple growth events during diamond genesis: an integrated study of carbon and nitrogen isotopes and nitrogen aggregation state in coated stones. *Earth Planet. Sci. Lett.*, **86**, 341–53.

Bragg, W. L. and Claringbull, G. F. (1965) *Crystal Structures of Minerals*, London, Bell and Sons.

Bruton, E. (1978) *Diamonds*, 2nd ed., N.A.G. Press, London.

Chang, L. L. Y. (1965) Subsolidus phase relations in the systems $BaCO_3$–$SrCO_3$, $SrCO_3$–$CaCO_3$ and $BaCO_3$–$CaCO_3$. *J. Geol.*, **73**, 346–68.

Chrenko, R. M., McDonald, R. S., and Darrow, K. A. (1967) Infra-red spectra of diamond coat. *Nature*, **213**, 474–6.

Cliff, G. and Lorimer, G. W. (1975) The quantitative analysis of thin specimens. *J. Microsc.*, **103**, 203–7.

Custers, J. F. H. (1950) On the nature of the opal-like outer layer of coated diamonds. *Am. Mineral.*, **35**, 51–8.

Graf, D. L. (1961) Crystallographic tables for the rhombohedral carbonates. Ibid., **46**, 1283–316.

Guthrie, G. D. Jr., Veblen, D. R., Navon, O., and Rossman, G. R. (1991) Submicrometer fluid inclusions in turbid-diamond coats. *Earth Planet. Sci. Lett.*, **105**, 1–12.

Harris, J. E. (1980) Recent research—the diamond geologists' tale. *Industrial Diamond Review*, **40**, 470–7.

Howie, R. A. and Broadhurst, F. M. (1958) X-ray data for dolomite and ankerite. *Am. Mineral.*, **43**, 1210–4.

Kamiya, Y. and Lang, A. R. (1965) On the structure of coated diamonds. *Phil. Mag.*, **11**, 347–56.

Kesson, S. E. and Ringwood, A. E. (1989) Slab-mantle interactions. 2. The formation of diamonds. *Chem. Geol.*, **78**, 97–118.

Lang, A. R. and Walmsley, J. C. (1983) Apatite inclusions in natural diamond coat. *Phys. Chem. Mineral.*, **9**, 6–8.

——Moore, M., and Walmsley, J. C. (1992) Diffraction and imaging studies of diamond. In *The Properties of Natural and Synthetic Diamond* (J. E. Field, ed.) Chapter 5, Academic Press, London.

Machado, W. G., Moore, M., and Woods, G. S. (1985) On the dodecahedral growth of coated diamonds. *J. Crystal Growth*, **71**, 718–27.

Meyer, H. O. A. (1987) Inclusions in diamond. In *Mantle Xenoliths* (P. H. Nixon, ed.), Wiley, New York, N.Y., pp. 501–22.

Navon, O., Hutcheon, I. D., Rossman, G. R., and Wasserburg, G. J. (1988) Mantle-derived fluids in diamond micro-inclusions. *Nature*, **335**, 784–9.

Orlov, Yu. L. (1977) *The Mineralogy of the Diamond*, Wiley, New York.

Touloukian, Y. S., Kirby, R. K., Taylor, R. E., and Lee, T. Y. R. (1977) *Thermal Expansion—Nonmetallic Solids, Thermophysical Properties of Matter*, Vol. 13, pp. 638–40, IFI/Plenum, New York–Washington.

Walmsley, J. C. (1981) *The nature of diamond coat.* M.Sc. Thesis, University of Bristol.

——and Lang, A. R. (1992a) Oriented biotite inclusions in diamond coat. *Mineral. Mag.*, **56**, 108–11.

————(1992b) Study of a platelet-free infilling of a crack in natural diamond: evidence for a late growth event. *J. Crystal Growth*, **116**, 225–34.